In situ synchrotron high-energy X-ray diffraction analysis on phase transformations in Ti–Al alloys processed by equal-channel angular pressing

Klaus-Dieter Liss,[a]* Ross E. Whitfield,[a] Wei Xu,[b] Thomas Buslaps,[c] LaReine A. Yeoh,[a] Xiaolin Wu,[b] Deliang Zhang[d] and Kenong Xia[b]*

[a]The Bragg Institute, Australian Nuclear Science and Technology Organisation, Private Mail Bag 1, Menai, NSW 2234, Australia, [b]Department of Mechanical Engineering and ARC Centre of Excellence for Design in Light Metals, University of Melbourne, Victoria 3010, Australia, [c]European Synchrotron Radiation Facility, BP 220, F-38043 Grenoble Cedex, France, and [d]Department of Materials and Process Engineering, University of Waikato, Hamilton, New Zealand. E-mail: kdl@ansto.gov.au, k.xia@unimelb.edu.au

Mixtures of 47-Al and 53-Ti powders (atomic %) have been consolidated using back pressure equal-channel angular pressing starting with both raw and ball-milled powders. *In situ* synchrotron high-energy X-ray diffraction studies are presented with continuous Rietveld analysis obtained upon a heating ramp from 300 K to 1075 K performed after the consolidation process. Initial phase distributions contain all intermetallic compounds of this system except Al, with distribution maxima in the outer regions of the concentrations (α-Ti, TiAl$_3$). Upon annealing, the phase evolution and lattice parameter changes owing to chemical segregation, which is in favour for the more equilibrated phases such as γ-TiAl, α_2-Ti$_3$Al and TiAl$_2$, were followed unprecedentedly in detail. An initial δ-TiH$_2$ content with a phase transition at about 625 K upon heating created an intermediate β-Ti phase which played an important role in the reaction chain and gradually transformed into the final products.

Keywords: Ti; Al; phase transformation; phase equilibria; powder metallurgy; structural; X-ray diffraction.

1. Introduction

The titanium–aluminium binary system is rich in intermetallic phases which may bear advantages as light-weight structural materials for applications at elevated temperatures or under mechanic load (Kim, 1995; Bartolotta & Krause, 1999; Yamaguchi *et al.*, 2000; Kestler & Clemens, 2003). Numerous metallurgical methods have been approached for their production, including casting, ingot metallurgy, powder metallurgy, cold spraying and reactive powder metallurgy (Kim, 1995). Most of them, however, produce materials with microstructures consisting of various phases at the micrometre-scale level. As ultrafine-grained and nanostructured metallic materials have exhibited superior mechanical properties over their coarse-grained counterparts (Wang *et al.*, 2002; Valiev & Langdon, 2006), it is of scientific and technological interest to explore a novel approach to fabricate such structured materials from TiAl-based alloys. Among techniques of producing ultrafine-grained and nanostructured materials, equal-channel angular pressing (ECAP) is very promising to effectively refine coarse grains into ultrafine or even nanoscale ones, and to produce fully dense bulk samples

(Valiev & Langdon, 2006). Since Ti–Al intermetallic materials are intrinsically brittle and difficult to process directly using ECAP, an alternative dual-step approach has been developed in this study, *i.e.* consolidation of elemental powders using back pressure (BP) assisted ECAP, which is effective in producing fully dense ultrafine and nanostructured Al (Xia & Wu, 2005; Xu *et al.*, 2007) and Ti (Xu *et al.*, 2008), followed by subsequent heat treatment to form intermetallic phases *via* phase transformations. It is therefore of great importance to explore the evolution of various phases upon heating using state-of-the-art characterization techniques such as *in situ* synchrotron high-energy X-ray diffraction analysis in the present study.

In situ X-ray diffraction has been applied since 1989 to the study of the phase evolution in titanium aluminides (Shull & Cline, 1989). Laboratory X-rays, however, suffer from insufficient penetration into metallic systems and lack of intensity. This has been overcome with the development of high-energy X-rays at modern synchrotron sources (Liss *et al.*, 2003). The intensities and energies of synchrotron X-rays allow information from the bulk of material to be followed on the one-second time scale while undergoing a heating cycle. Recently,

825

high-temperature phases have been verified *in situ* (Clemens *et al.*, 2008) and the phase evolution has been followed and evaluated by quantitative Rietveld analysis revealing transition temperatures and phase compositions, but also order and disorder in the crystallographic systems (Yeoh *et al.*, 2007). Furthermore, this method employs acquisition by a two-dimensional detector, which allows additional information, such as grain correlations and their statistics, to be extracted (Liss *et al.*, 2006, 2007*a*,*b*, 2008, 2009). With this background, the *in situ* diffraction technique is applied for the first time to the quantitative investigation of the above-mentioned reaction synthesis of BP-ECAP consolidated Ti–Al material, in order to reveal in detail the evolution of phase composition, lattice parameters and crystallographic order and disorder upon *in situ* heating.

2. Experimental materials and procedures

Two types of Ti–Al powders were prepared for subsequent consolidation. The first consists of mechanically stir-mixed pure Al and Ti elemental particles of composition Ti–47Al (all in atomic %). The atomized Al powder comprises particles of irregular shape with a mean size of ∼35 µm (Xia & Wu, 2005), and the crushed Ti particles, also of irregular shape, were coarser with a mean size of ∼96 µm (Wu & Xia, 2006). The second is a ball-milled Ti–Al powder (Zhang, 2004) of Ti–47Al produced from pure Al and Ti particles with average sizes of 70 µm and 150 µm, respectively. The milling took place at room temperature for 24 h in a centrifugal mill with a ball to powder weight ratio of 10:1 under high-purity Ar atmosphere and without using any process control agent. The examination of the as-milled powder revealed Ti particles embedded in Al with no formation of any compounds between Ti and Al. X-ray analysis indicates that the Ti and Al grains in the as-milled powder are reduced to the submicrometre range.

The consolidation of the powders was carried out by using BP-ECAP. The set-up has been described in detail elsewhere (Xia & Wu, 2005). The two channels of the ECAP die intersect at 90° with equal cross sections of 9 mm × 9 mm and back pressure could be applied through a back plunger in the exit channel. The powder to be consolidated was wrapped in Al foil and placed in the entrance channel with graphite lubrication. The assembled die set was heated to 903 K by surrounding heating elements and controlled to ±1 K through a thermocouple near the outer corner of the channel intersection. After stabilizing at the temperature for 15 min, pressing was conducted at a speed of 0.2 mm min^{-1} with a constant back pressure of 200 MPa. The material consolidated from the mechanically stir-mixed powder is designated as the raw, and that from the milled powder as the milled or ball-milled in the following text.

Cylindrical samples of diameter 4 mm and height 10 mm were taken from the middle of the consolidated materials for *in situ* high-energy X-ray diffraction studies (Liss *et al.*, 2003) at beamline ID15B of the European Synchrotron Radiation Facility (ESRF) in Grenoble (Liss *et al.*, 2006, 2007*a*,*b*, 2008). The novel Thales Pixium 4700 flat-panel pixel detector (Daniels & Drakopoulos, 2009) was used for fast data acquisition, here with 1 s exposure time every 10 s. The X-ray energy, wavenumber, detector distance and pixel size of the beamline were calibrated with a Fe standard to 88.95 keV, 45.08 Å^{-1}, 1162 mm and 0.154 mm, respectively. A cylindrical furnace with openings for the X-ray beams was used to control the temperature with an input of helium flow to reduce oxidation. Special care was taken for the sample mount which consisted of a hollow alumina stick and a collar with an inner diameter of 4 mm at the top end to hold the sample sitting in direct contact with the incorporated type-S thermocouple. The temperature profile run on both the raw and the ball-milled samples was as follows: heating from room temperature to 875 K at 5 K min^{-1}, heating from 875 to 1075 K at 3 K min^{-1}, holding at 1075 K for 10 min, and cooling to room temperature at 5 K min^{-1}. The data acquisition started at 360 K and 310 K on heating and finished at 515 K and 595 K on cooling, lasting 5.10 h and 4.75 h, for the milled and raw samples, respectively.

The Rietveld analysis was used for whole powder-diffraction pattern fitting to obtain quantitative values of the phase fractions and lattice parameters throughout the *in situ* experiments. The original two-dimensional diffraction patterns were reduced using the *dataRring* package (Yeoh & Liss, 2006) which automatically locates and fits the centre of the Debye–Scherrer rings and subsequently integrates along azimuthal sectors, in the present case the full circle, binning intensity values linearly into three independent quantities, namely image-radius (pixels), reciprocal lattice units (Q) and conventional scattering angle (2θ). The package is fully scriptable and based on the *SCILAB* platform (http://www.scilab.org/) which allows for mass data reduction on typically a few thousand image files per temperature run. The freely available Rietveld programs *GSAS* with *EXPGUI* (Larson & Von Dreele, 2000; Toby, 2001) and *MAUD* (Lutterotti, 2005) were chosen to run on Linux in order to employ further batch processing. Initially, *GSAS* with *EXPGUI* was used to fit some patterns to give consistency and better fitting. *MAUD* was employed later for the batch runs as it modelled the phase transitions better without diverging. For any time, each one-dimensional diffraction pattern was subsequently fed into Rietveld analysis to produce quantitative results, *i.e.* the phase fractions and lattice parameters as a function of time or temperature. The Rietveld analysis started by setting up *MAUD* with a well fitted analysis file which was then used for recursive fitting of the following data file differing by only a little (Lutterotti, 2005). The batch running was repeated several times with different starting values and constraints to start the iterating process until there was a consistently good fit throughout the entire run.

Examples of batch Rietveld refined patterns for the raw material are given in Fig. 1 before (*a*) and after (*b*) the phase transformation occurring at 630 K, at which basically the δ-TiH$_2$ phase disappears and β-Ti appears. The Rietveld R-factors are 5.96% and 6.87%, respectively. It should be noted that these refinements are not as good as could be achieved if each was done separately. The refinements were checked at
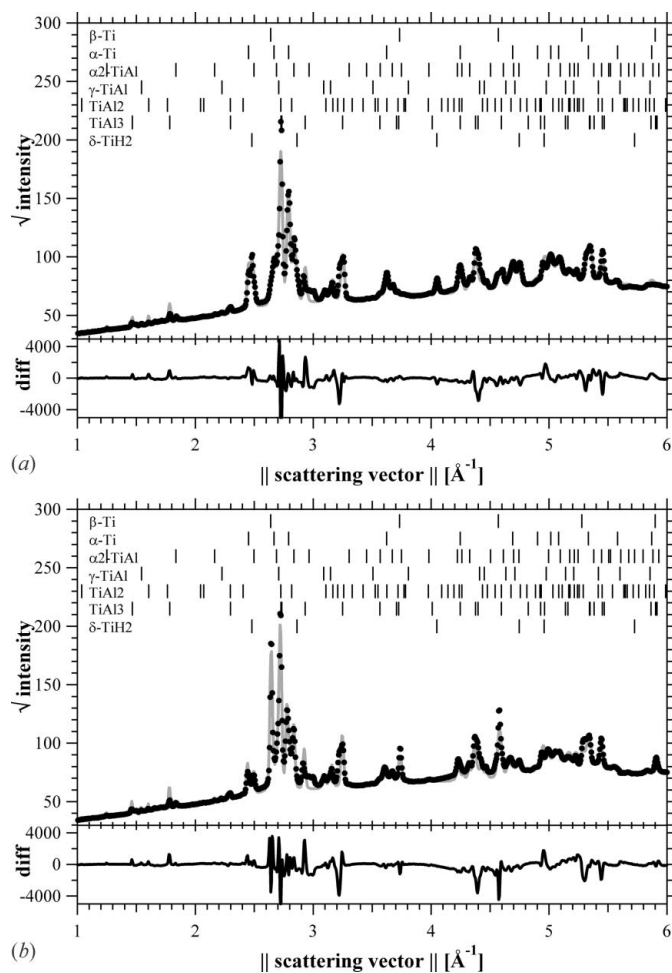
(a)

(b)

Figure 1
Rietveld results from the batch run on the raw sample (a) before and (b) after the phase transformation occurring at 630 K. The main graph shows the experimental data (dark dots) on top of the fitted curve (grey line). The residual between computed and experimental data is depicted in the bottom graphs. Refined peak positions for the different phases are given at the top.

various points by additional refinement of single patterns using both *MAUD* and *GSAS* with results close to that found using the batch refinement.

3. Experimental results

The two-dimensional diffraction rings were reduced to one-dimensional powder diffraction patterns as depicted in Figs. 2 and 3 for the ball-milled and raw samples, respectively. One selected profile of each is shown at the bottom of the figures while the time evolution is given in the upper part, intensity being coded in greyscale. Thus, the selected pattern represents one horizontal line at given time in the upper image. The temperature profiles are overlaid to the right of the images with the common time axis. Phase fractions from the Rietveld analysis are shown in Figs. 4 and 5 for the milled and raw materials, respectively. Seven phases related to the Ti, Ti–Al and Ti–H systems, namely β-Ti, α-Ti, α_2-Ti$_3$Al, γ-TiAl, TiAl$_2$,
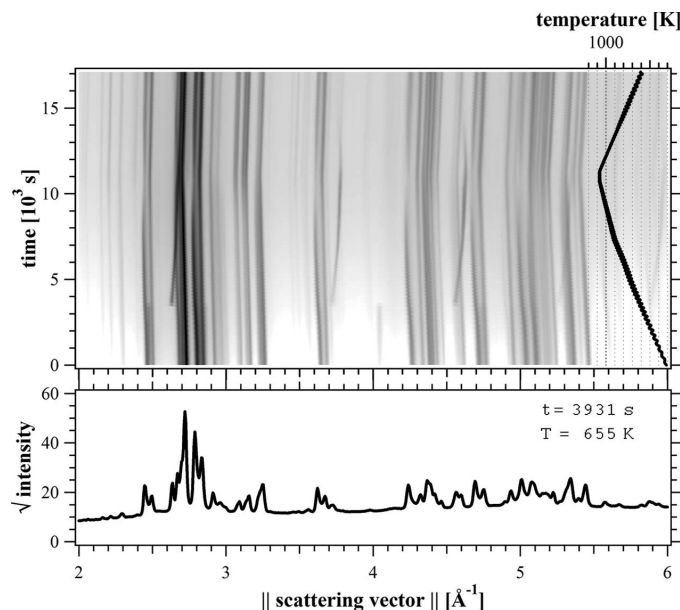

Figure 2
Powder diffraction patterns showing intensity *versus* scattering vector obtained from the two-dimensional diffraction rings at $t = 3931$ s or $T = 655$ K (bottom), and the greyscale-coded pattern revealing the time evolution of phases during the entire temperature scan (top) for the ball-milled sample.
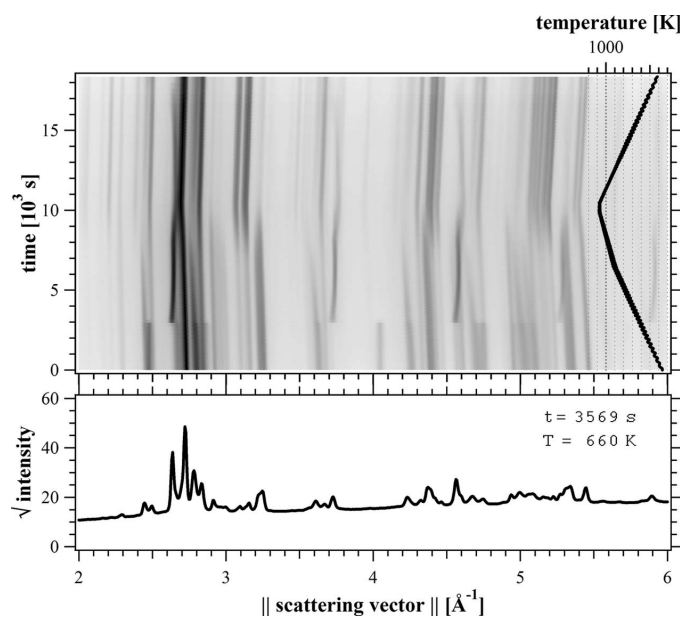

Figure 3
Powder diffraction patterns showing intensity *versus* scattering vector obtained from the two-dimensional diffraction rings at $t = 3569$ s or $T = 660$ K (bottom), and the greyscale-coded pattern revealing the evolution of phases during the entire temperature scan (top) for the raw sample.

TiAl$_3$ and δ-TiH$_2$, were identified in both the ball-milled and the raw samples. After careful comparison with the observed lines an extra α-Ti phase with slightly distinct lattice parameters was introduced into the raw sample, presumably one without and one with higher concentration of Al. This phase is designated as α-Ti(Al) in the following text. These eight

Table 1
Phases identified in the raw and milled samples and their structures and lattice parameters.

The measured values were obtained close to room temperature while the β-Ti values had been taken just above the phase transformation at 630 K.

| Phase	Formula	Structure		Literature (Schuster & Palm, 2006)		Ball milled – measured		Raw mixed – measured	
				a	c	a	c	a	c
α	Ti	$P6_3/mmc$	h.c.p.	2.9506	4.6835			2.9451873	4.700645
α	Ti(Al)	$P6_3/mmc$	h.c.p.			2.9407275	4.674912	2.9421873	4.700645
α_2	Ti$_3$Al	$P6_3/mmc$	Hexagonal	5.765	4.625	5.792411	4.6421256	5.7947116	4.6586237
β	Ti	$Im\bar{3}m$	b.c.c.	3.3065		3.3731685 (630 K)		3.3675938 (630 K)	
γ	TiAl	$P4/mmm$	Tetragonal	4.000	4.075	3.9881074	4.0637126	3.9823837	4.0534835
TiAl2	TiAl$_2$	$I4_1/amd$	Tetragonal	3.971	24.312	3.9599948	24.237858	3.9589262	24.180155
TiAl3	TiAl$_3$	$I4/mmm$	Tetragonal	3.849	8.61	3.8485966	8.572131	3.8561616	8.545578
δ	TiH$_2$	$Fm\bar{3}m$	f.c.c.	4.431		4.39		4.39	
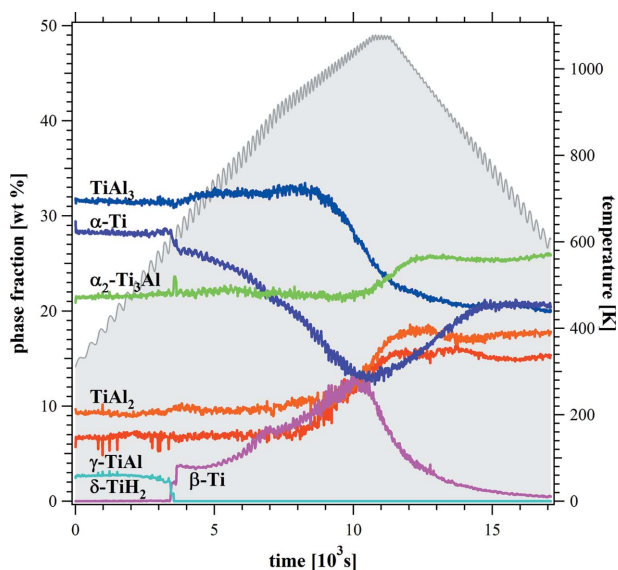
Figure 4
Weight fractions of the detected phases as a function of time (temperature) during the *in situ* scan as obtained by Rietveld refinement analysis in the ball-milled sample.
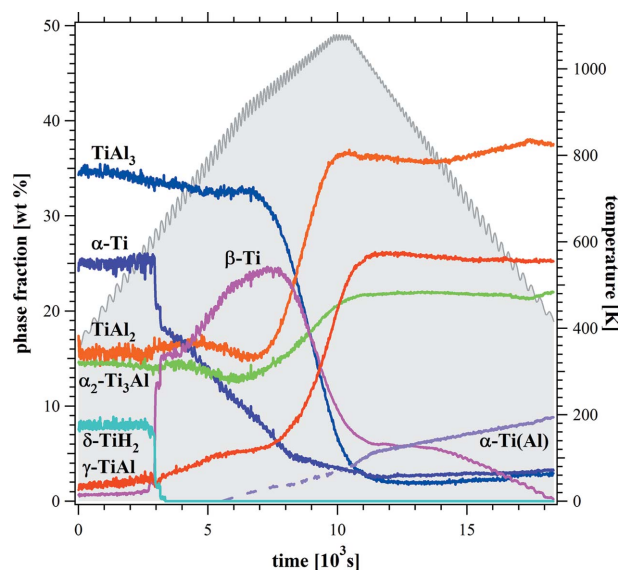

Figure 5
Weight fractions of the detected phases as a function of time (temperature) during the *in situ* scan as obtained by Rietveld refinement analysis in the raw sample.

phases are listed in Table 1 with their structures and references and measured lattice parameters.

The presence of these phases was verified by comparison with the corresponding greyscale-coded pattern. It is obvious that the f.c.c. Al phase in the initial powders were all consumed by forming TiAl$_3$, TiAl$_2$, γ-TiAl, α_2-Ti$_3$Al and α-Ti(Al). The presence of these phases in the Ti–Al system is underlined by the strong peak around 2.72 Å^{-1}, indicating that they all have similar spacings between close-packed planes, and mostly local rearrangements and ordering distinguishes them. It is also clear that phase transformations occur throughout the temperature scan, resulting in changes in the phase fractions, disappearance of some phases and emergence of others. The phase fractions of the Ti–Al system existing before and after the *in situ* cycle are schematically plotted against the Al content in Figs. 6 and 7 with the phases identified.

Although all the intermetallic phases and the α-Ti or α-Ti(Al) phase were present in the as-ECAP consolidated materials, the compounds with higher asymmetric atomic ratios (*i.e.* Ti, Ti$_3$Al, TiAl$_3$) are more represented than the

symmetric TiAl. At the end of the temperature cycle the amount of TiAl was significantly increased, especially for the raw sample which contained very little TiAl at the beginning. Owing to their larger sizes in the raw material, initial α-Ti particles partly remained after ECAP, as evidenced by the lattice parameter ($a = 2.9452$ Å) compared with the literature value ($a = 2.9506$ Å) as shown in Table 1. In contrast, the α-Ti(Al) contains up to $\sim$10 at% of Al, resulting in a shorter lattice parameter ($a = 2.9422$ Å). In the ball-milled sample, the α-Ti and α-Ti(Al) samples cannot be distinguished. Although the relative difference between α-Ti and α-Ti(Al) is only 10^{-3}, it can be distinguished from systematic errors since it is measured simultaneously on the same sample. The difference from the literature values is more affected and it is difficult to put the results onto an absolute scale. For the c-axes of α-Ti(Al), we cannot loosen the fit parameter as there are too many reflections overlapping. Therefore, in a first approximation, we work with constant c values.

In addition to the Ti–Al-based phases, δ-TiH$_2$ was detected in the two as-ECAP processed materials, as shown in Figs. 4 and 5. This titanium hydride phase was completely trans-
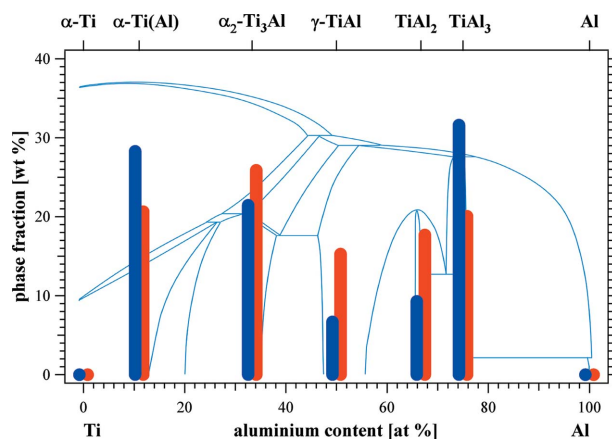
Figure 6
Fractions of the phases against the Al content in the Ti–Al system existing before (blue bars) and after (red bars) the *in situ* temperature cycle in the ball-milled sample. The phase diagram is superimposed for schematic orientation.
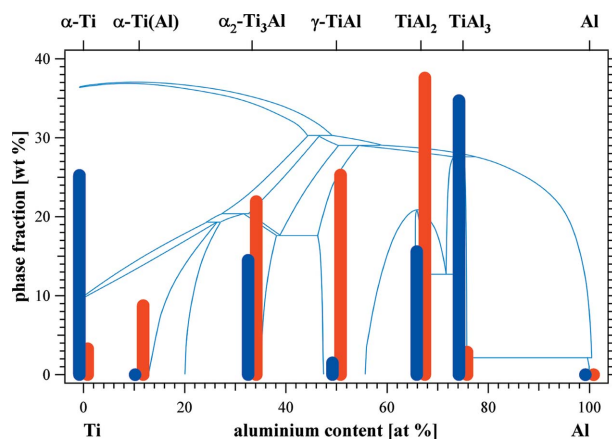

Figure 7
Fractions of the phases against the Al content in the Ti–Al system existing before (blue bars) and after (red bars) the *in situ* temperature cycle in the raw sample. The phase diagram is superimposed for schematic orientation.

formed into β-Ti at about 630 K in both cases, although the b.c.c. structured β-Ti had a larger lattice parameter with $a = 3.37$ Å compared with 3.30 Å in the literature, as shown in Table 1, and a higher transition temperature, which is 571 K in the literature (San-Martin & Manchester, 1987; Manchester & San-Martin, 2000). The amount of the β-Ti phase reached the maximum at around the peak temperature of 1075 K in the ball-milled sample and at ~950 K in the raw sample; it then decreased to complete disappearance during cooling.

The other information that can be readily extracted from the diffraction data is the lattice parameters. The variations of the lattice parameters relevant to each of the Ti/Ti–Al-based structures during the temperature cycle are plotted in Figs. 8 and 9 for the ball-milled and raw materials, respectively. It is noted that the curves during heating do not always overlap with those during cooling. Further, for the hexagonal and tetragonal structured phases, the c/a ratios are normalized to

those for the corresponding close-packed structures, and their changes with temperature during heating and cooling are plotted in Figs. 10 and 11 for the ball-milled and raw materials, respectively. Again, large differences were observed during heating and cooling.

4. Discussion

4.1. Non-equilibrium towards equilibrium

Based on the equilibrium phase diagram (Schuster & Palm, 2006), Al and Ti would react to form a series of ordered intermetallics including TiAl$_3$, TiAl$_2$, TiAl and Ti$_3$Al, in addition to a solid solution α-Ti(Al) at the Ti-rich end. Both the mechanically mixed raw and ball-milled powders consisted of only the starting Al and Ti phases and were thus highly non-equilibrium. The ECAP was conducted at a temperature which was expected to result in the reactions between Ti and Al. Indeed, after consolidation at 903 K by BP-ECAP and at the beginning of the present *in situ* experiment, Al and Ti had inter-diffused into each other and formed TiAl$_3$ and TiAl$_2$ on the Al side and α-Ti(Al), Ti$_3$Al on the Ti side, and eventually γ-TiAl in the centre of the phase diagram. The reaction kinetics, however, not only depends on the temperature and time of ECAP, but also on the diffusion distance. The average sizes of Al and Ti particles in the raw material were ~35 µm and 96 µm, respectively, while the milled powder showed reduced dimensions in the submicrometre range between Al and Ti layers. That is to say, the diffusion distances on average were much shorter in the ball-milled sample than in the raw sample. Indeed, only a very small fraction of ~2 wt% of TiAl was formed in the raw material, compared with that in the ball-milled sample with ~8%. Together with the fact that Ti particles were bigger than the Al ones in the raw material, much of the α-Ti was not consumed with 25% left whereas all Al had been transformed into intermetallic compounds. Moreover, the α-Ti in the ball-milled sample contained a high content of Al in solid solution, compared with the pure α-Ti in the raw sample.

After the *in situ* temperature cycle, γ-TiAl, TiAl$_2$ and α_2-Ti$_3$Al increased in amount at the expense of TiAl$_3$ and α-Ti in both materials although α-Ti(Al) remained significantly present in the ball-milled material and was newly formed in the raw sample. In particular, the transition from TiAl$_3$ to γ-TiAl, TiAl$_2$ and Ti$_3$Al became obvious at ~950 K upon heating and stopped at just past the peak temperature of 1075 K in both materials, as shown in Figs. 4 and 5. The behaviour underlines the fact that the reaction to the end products takes place at increased temperatures, while the back transformation is not observed upon cooling. Most of the product phases then remain constant and only the β-Ti phase will transform at lower temperatures. It is suggested that further transformation will take place at even higher temperatures or longer holding times.

Phase evolutions similar to those in the present study were also reported in Ti–Al alloys prepared by reactive hot pressing and self-propagating high-temperature synthesis of the
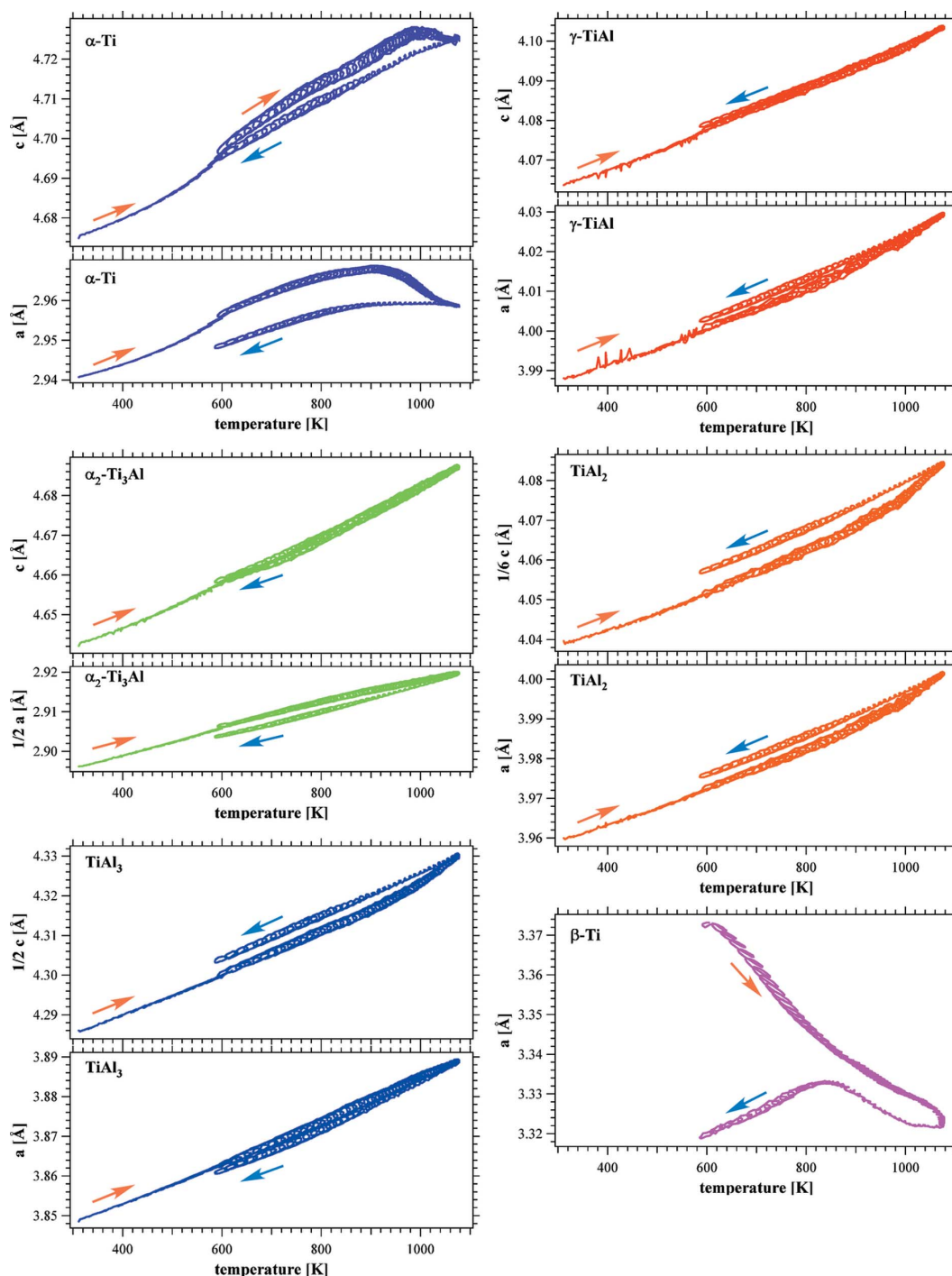
Figure 8
Change of the relevant lattice parameters during heating and cooling in various Ti/Ti–Al phases in the ball-milled sample.

blended powders of elemental Ti and Al particles (Paransky *et al.*, 1996; Rawers & Wrzesinski, 1992; Yang & Weatherly, 1996; Fang *et al.*, 2005). For instance, hot pressing of a Ti–50Al (atomic %) blended powder at 973 K yielded all the apparent intermetallic phases including Ti_3Al, $TiAl$, $TiAl_2$ and $TiAl_3$ and with the presence of a large amount of unreacted Ti (Paransky *et al.*, 1996), *i.e.* the microstructure was highly non-equilibrium. Pressing at a higher temperature of 1173 K led to the formation of a microstructure closer to equilibrium,

consisting of Ti_3Al, $TiAl$ and $TiAl_2$ phases. However, post heat treatment at even higher temperature (*e.g.* 1373 K) was required to reach an equilibrium microstructure of mainly $TiAl$ (Paransky *et al.*, 1996). In addition, during self-propagating high-temperature synthesis it was reported that $TiAl_3$ was always the first phase to form followed by $TiAl$ and Ti_3Al, irrespective of the starting composition (Yang & Weatherly, 1996), which is consistent with the observations in the present study (Figs. 4 and 5).
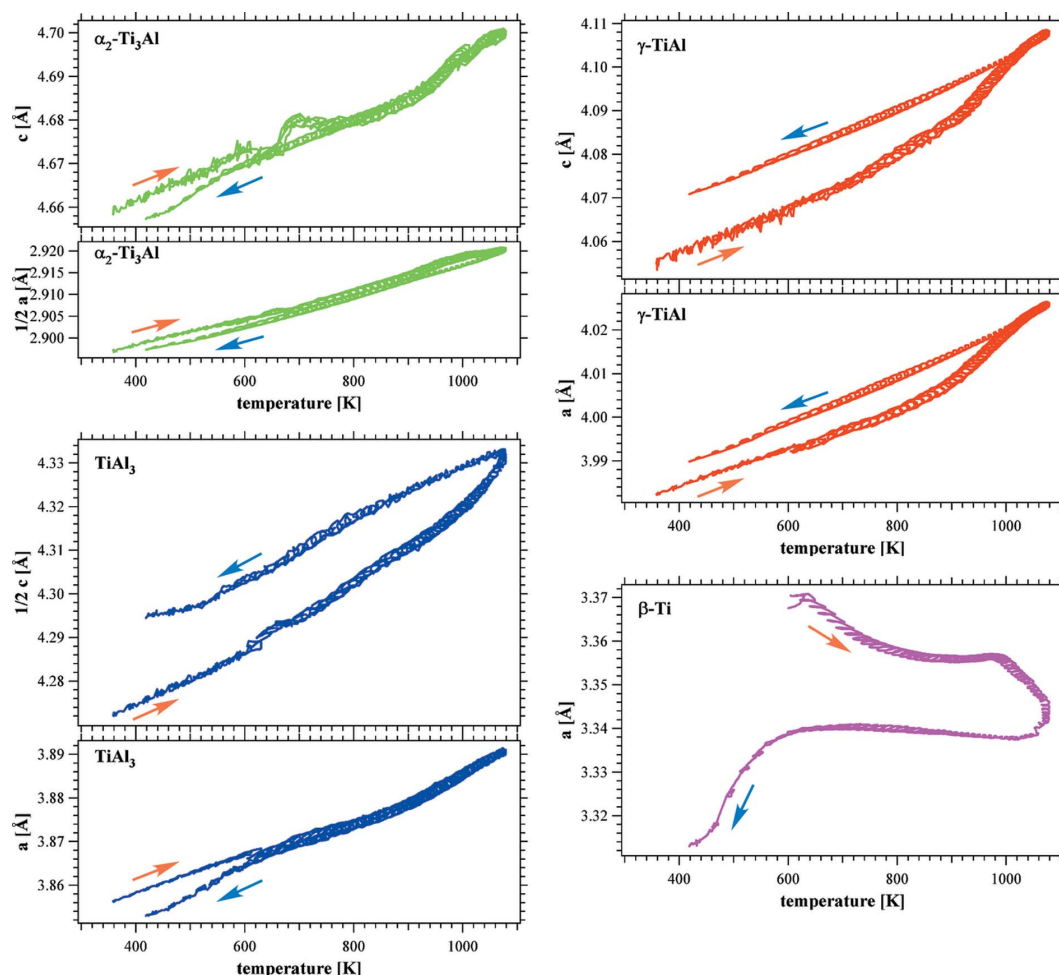
Figure 9
Change of the relevant lattice parameters during heating and cooling in various Ti/Ti–Al phases in the raw sample.

4.2. Formation of β-Ti at 630 K

The presence of δ-TiH$_2$ in the as-ECAP processed materials and its disappearance with the formation of β-Ti at $\sim$630 K are interesting and deserve further analysis. First of all, it is known that pure Ti absorbs hydrogen from the atmosphere (Wasz *et al.*, 1996). The powders used were not dehydrogenated before processing and thus expected to contain some amounts of δ-TiH$_2$. From Figs. 4 and 5 it is apparent that this phase suddenly disappeared at $\sim$630 K, accompanied by the sudden appearance of β-Ti and decrease in α-Ti(Al) in the ball-milled sample and α-Ti, more dramatically, in the raw sample. Differential scanning calorimetry analysis confirmed a phase transition starting at $\sim$600 K. According to the Ti–H phase diagram (Manchester & San-Martin, 2000; Domizzi *et al.*, 2006) there is a eutectoid reaction, δ-TiH$_2$ + α-Ti $\leftrightarrow$ β-Ti, at 571 K. Quantitatively, the fraction changes of the three phases at 630 K in the raw sample are observed according to this law (Fig. 5): (8.2% δ-TiH$_2$) + (7.1% α-Ti) $\rightarrow$ (15.1% β-Ti), indicating that such a reaction had indeed taken place. The reported eutectoid temperature of 571 K, however, is 59 K below the observed value of 630 K. This apparent discrepancy might be explained by the increase in volume related to the transformation and the strong pressure dependence of the phase transition (Shen & Perng, 2007). During ECAP, the high back pressure of 200 MPa prevented the formation of the higher-volume β-Ti even though the process temperature of 903 K was well above 571 K. During the subsequent heating, the surrounding matrix still restricts the volume expansion associated with the reaction, shifting the observed transition temperature up.

The occurrence of such a reaction is further supported by observing the lattice parameter changes in δ-TiH$_2$ and β-Ti. The stoichiometric δ-TiH$_2$ containing 66.7 at% H has a lattice parameter of a = 4.431 Å with Ti forming the f.c.c. structure and H occupying all the tetrahedral interstitial sites (Irving & Beevers, 1971). A metastable hypothetic δ-Ti phase of f.c.c. structure which differs from α-Ti by its stacking sequence along c would have a lattice constant of $a_{fcc} = \sqrt{3}/2\,c_{hcp}$ = 4.06 Å and has indeed been predicted by first-principle calculations (Ghosh & Asta, 2005). Such a δ-Ti would show the same structure as the δ-TiH$_2$ without H. Based on the Ti–H phase diagram, the δ-TiH$_2$ in equilibrium with α-Ti should have a non-stoichiometric composition containing $\sim$60 at% H, *i.e.* some of the tetrahedral interstitial sites were not occupied. Linear interpolation using Vegard's law (Denton &
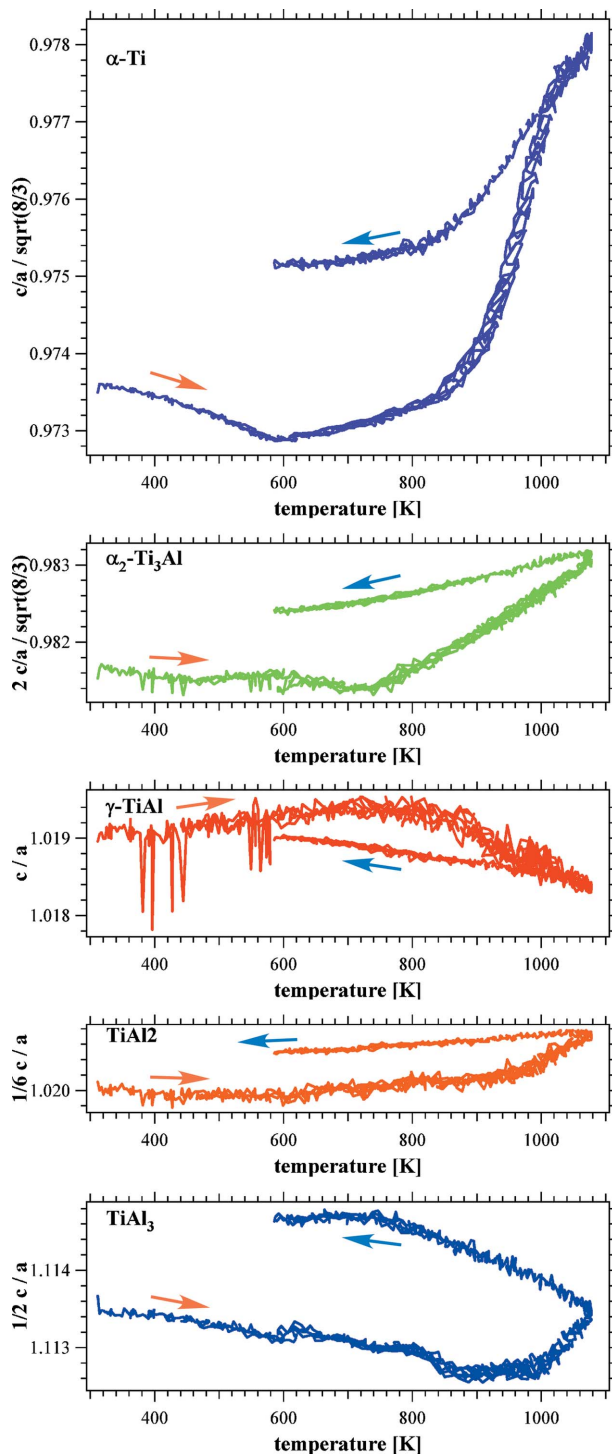
Figure 10
Change of the *c/a* ratios normalized to those of the corresponding close-packed structures during heating and cooling in the hexagonal and tetragonal structured phases in the ball-milled sample.

Ashcroft, 1991) led to a predicted lattice parameter of $a = 4.39$ Å, matching perfectly the value observed in the two materials (Table 1). The composition of the β-Ti formed from the reaction can be estimated from the eutectoid composition of the phase diagram to be around 42.5 at% H, leading to a larger lattice parameter of ~ 3.37 Å compared with pure β-Ti
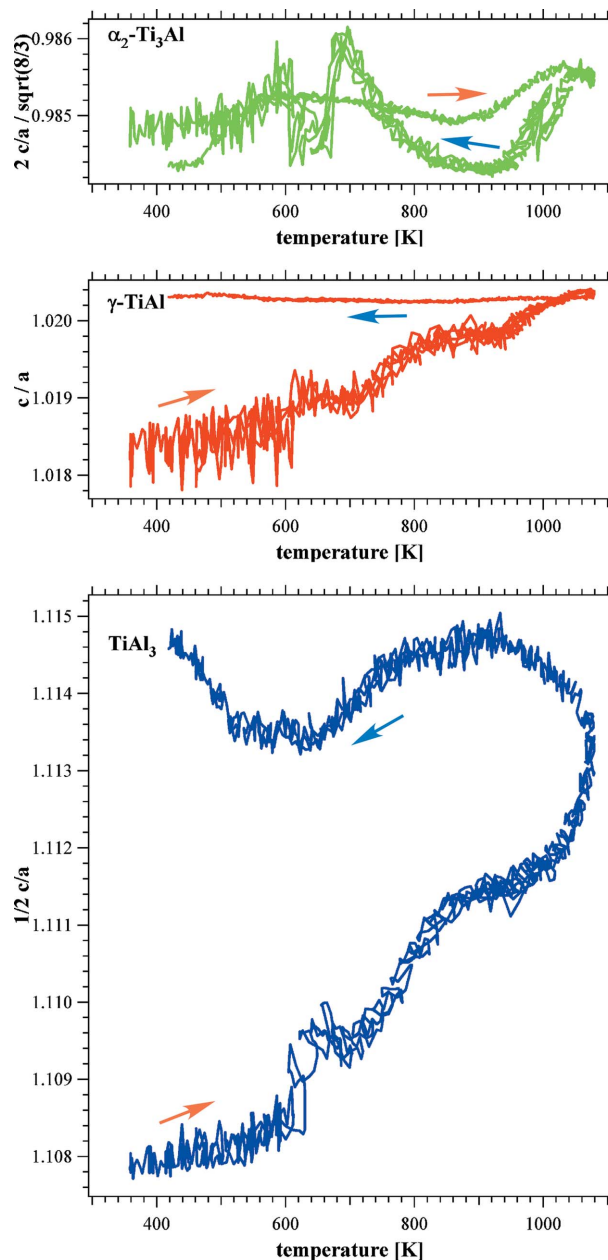

Figure 11
Change of the *c/a* ratios normalized to those of the corresponding close-packed structures during heating and cooling in the hexagonal and tetragonal structured phases in the raw sample.

with ~ 3.30 Å as shown in Table 1 and observed by Senkov *et al.* (2001).

4.3. α-Ti $\leftrightarrow$ β-Ti transformations after 630 K

Although δ-TiH$_2$ disappeared completely at 630 K, the newly formed β-Ti continued to change and interacted with the evolution of the other phases during further heating to the peak temperature of 1075 K. In particular, the fraction of β-Ti increased and that of α-Ti decreased simultaneously until 1075 K while the other phases remained relatively unchanged up to ~ 950 K. This implies that α-Ti was continuously trans-

formed into β-Ti even after all δ-TiH$_2$ had been consumed. This can be understood by referring to the Ti–H phase diagram (Domizzi *et al.*, 2006) (the temperatures were higher though, as explained in §4.2). As temperature increases, β-Ti dissolves less H to be stable, *i.e.* the composition of β-Ti follows the β transus line in balance with α, and the excess H was transferred to the existing α-Ti phase, resulting in the formation of more β-Ti.

The decrease of H content in the β-Ti phase with increasing temperature is consistent with the change in its lattice parameter. In the simplest case, changes in lattice parameters were only related to thermal expansion, as demonstrated by the change of $c|_\gamma$ for the γ phase in the ball-milled sample (Fig. 8), which followed a linear relationship and, more importantly, superimposes during heating and cooling. For the β-Ti phase, however, the lattice parameter $a|_\beta$ shrank considerably during heating until the maximum temperature was reached. In other words, the effect of H reduction in β-Ti as discussed above, which caused a decrease in the lattice parameter (Senkov *et al.*, 2001), was more significant than that of thermal expansion, resulting in net shrinking. Although this 'shrinking on heating' was observed in both materials, the kinetics was probably slower in the raw material owing to greater diffusion distances. In fact, the fraction of β-Ti reached maximum when the other intermetallic phases started to be formed at ∼950 K (Fig. 5). In other words, there was less formation of β-Ti in the raw material, and this in turn would lead to less dilution of the concentration of H, reducing its contribution to the change in the lattice parameter. Indeed, the shrinking became less significant.

During cooling, the transformation was reversed, *i.e.* β-Ti was converted into α-Ti, as seen in Fig. 4 for the ball-milled material. As the temperature dropped, there was less β-Ti containing a higher concentration of H, resulting in an increase in the lattice parameter (Senkov *et al.*, 2001). This effect was initially stronger than that of thermal shrinking, leading to an increase in the lattice parameter. The β to α transformation became insignificant at ∼800 K, and the lattice parameter decreased following the simple thermal shrinking below this temperature as seen in Fig. 8. The situation was again slightly different in the raw material where the transformation back into α was less pronounced initially on cooling (Fig. 5), *i.e.* the effect of H concentration has been smaller than in the ball-milled sample. Consequently, a plateau was observed, rather than an increase in the lattice parameter, before simple thermal shrinking took over as displayed in Fig. 9.

4.4. Evolution of the lattice parameters

As already discussed previously for the β-Ti and δ-TiH$_2$ phases, the crystallographic lattice parameters as well as their anisotropic behaviour given in c/a ratios are very sensitive to the stoichiometry and order/disorder of the structure. Previous studies have evaluated those for the two-phase system α_2-Ti$_3$Al and γ-TiAl (Yeoh *et al.*, 2007). The present results from the Rietveld refinement are given in Figs. 8 and 9

for the lattice parameters and in Figs. 10 and 11 for the corresponding c/a ratios. Owing to fitting divergences, constraints and profile overlapping, no representative curves were obtained for some phases of the raw sample. Some of the remaining kinks and glitches have to be interpreted with caution although the tendency during the evolution is shown. The fitting for the ball-milled sample was easier and more straightforward.

Mostly, the slope of the lattice parameters is governed by thermal expansion, and, if this was the only contribution, heating and cooling curves would overlap. Any discrepancies between the heating and cooling ramps are attributable to phase evolution, while details can be worked out following the *in situ* study. Generally, it can be stated that the phase evolution in the raw sample is stronger than that in the milled sample, confirming that the latter has already reacted further towards the equilibrium state during BP-ECAP.

The lattice parameters, a and c, of α-Ti for the ball-milled sample (Fig. 8) deviate from the general slope above 900 K whereas the c/a ratio upon heating and cooling is almost parallel but offset between 600 K and 800 K (Fig. 10). This can be understood by the uptake of Al into the Ti-rich α-Ti(Al) phase as the lattice parameters shrink with higher Al concentrations (Table 1). Similarly, the lattice parameters for the γ-TiAl increase as expected with an increase in Ti concentration when interpolating from the smaller Al to the larger δ-Ti lattice, both of f.c.c. structure (Ghosh & Asta, 2005). The c/a ratio of the γ-TiAl shrinks little but differs significantly between heating and cooling (Fig. 10). This indicates that slightly more disorder is introduced into the phase. Indeed, it has been reported that thermally induced disorder in a near-equilibrium γ-TiAl phase increases towards the eutectoid temperature of 1476 K (Yeoh *et al.*, 2007), and the order does not recover upon cooling owing to a relatively fast cooling rate. In contrast, γ-TiAl of the raw sample evolves with significantly smaller lattice parameters while the corresponding c/a ratio dramatically increases upon heating and remains constant upon cooling (Fig. 11). First of all, the initial phase fraction of γ-TiAl was only 2 wt% which suggests that the phase is far from equilibrium. Since the near-f.c.c. γ-TiAl structure is close to the Al structure, we attribute the smaller lattice parameters to a supersaturated concentration of Al, which is equivalent to higher disorder and consistent with the smaller c/a ratio. As the phase transformations and the chemical reactions evolve, the newly created γ-TiAl is more stoichiometric and ordered.

Similarly, TiAl$_3$ is another superstructure based on the f.c.c. unit cell, the unit repetition doubled along c. It is an ordered structure between γ-TiAl, TiAl$_2$ and pure Al. Therefore, as above, c/a of the near-f.c.c. unit should approach 1 when fully disordered and approach a maximum value with full order. Indeed, both c/a values approach the same value of 1.1147 (= $c/2a$) at the end of the *in situ* temperature treatment. However, they start from very different values, showing that the atomic disorder in the raw sample was sensitively higher than in the ball-milled specimen. The same tendency is observed for TiAl$_2$.

5. Summary and conclusions

In situ synchrotron high-energy X-ray diffraction was used to study the evolution of phases during heating and cooling in two Ti–Al alloys consolidated from ball-milled and mechanically stir-mixed powders, respectively, by back pressure equal-channel angular pressing at 903 K. Both powders consisted of just Al and Ti phases before consolidation although the phases were finer and better mixed in the ball-milled powder.

During consolidation, the original Al and Ti phases in the powders reacted to form various intermetallic compounds as well as α-Ti(Al) solid solution while all Al had been consumed. However, the phases were dominantly out of equilibrium with little formation of the equilibrium γ-TiAl especially in the coarser raw material after the consolidation.

During the *in situ* heating and cooling, the more equilibrium phases γ-TiAl, TiAl$_2$ and Ti$_3$Al gained at the expense of the highly non-equilibrium TiAl$_3$ and α-Ti. However, the march towards equilibrium was more significant in the raw sample, with a lower transformation starting temperature, than in the milled sample, leading to a phase structure closer to equilibrium despite an initially less equilibrium one

In addition, there was the δ-TiH$_2$ phase in both consolidated materials owing to absorption of H. This hydride phase reacted with α-Ti to form β-Ti at $\sim$630 K. The transformation from α to β continued above 630 K with a decrease in the H content in β which caused a reduction of the lattice parameter. The transformation was reversed to that of β to α on cooling until all the β was consumed.

The evolution of lattice parameters and their ratios bespeak the chemical order of the phases. This allows the behaviour of the H concentration in the β-Ti phase, the solution of Al in the α-Ti phase as well as the order/disorder of α_2-Ti$_3$Al and γ-TiAl to be followed in detail, leading to deeper insight into the kinetics of the multiphase system.

References

Bartolotta, P. A. & Krause, D. L. (1999). NASA Report NAS 1.15209071; NASA Report TM-1999–209071, pp. 3–10. NASA, USA.

Clemens, H., Chladil, H. F., Wallgram, W., Zickler, G. A., Gerling, R., Liss, K. D., Kremmer, S., Guther, V. & Smarslyg, W. (2008). *Intermetallics*, **16**, 827–833.

Daniels, J. E. & Drakopoulos, M. (2009). *J. Synchrotron Rad.* **16**, 463–468.

Denton, A. R. & Ashcroft, N. W. (1991). *Phys. Rev. A*, **43**, 3161–3164.

Domizzi, G., Luppo, M. I. & Vigna, G. (2006). *J. Alloys Compd.* **424**, 193–198.

Fang, W. B., Hu, L. X., He, W. X., Wang, E. D. & Li, X. Q. (2005). *Mater. Sci. Eng. A*, **403**, 186–190.

Ghosh, G. & Asta, M. (2005). *Acta Mater.* **53**, 3225–3252.

Irving, P. E. & Beevers, C. J. (1971). *Metallurg. Trans.* **2**, 613–618.

Kestler, H. & Clemens, H. (2003). *Titanium and Titanium Alloys*, pp. 351–392. Weinheim: Wiley-VCH.

Kim, Y. W. (1995). *J. Miner. Met. Mater. Soc.* **47**, 38.

Larson, A. C. & Von Dreele, R. B. (2000). *General Structure Analysis System (GSAS)*. Report LAUR 86–748. Los Alamos National Laboratory, USA.

Liss, K.-D., Bartels, A., Clemens, H., Bystrzanowski, S., Stark, A., Buslaps, T., Schimansky, F.-P., Gerling, R. & Schreyer, A. (2007*a*). *Mater. Sci. Forum*, **539–543**, 1519–1524.

Liss, K.-D., Bartels, A., Clemens, H., Bystrzanowski, S., Stark, A., Buslaps, T., Schimansky, F.-P., Gerling, R., Scheu, C. & Schreyer, A. (2006). *Acta Mater.* **54**, 3721–3735.

Liss, K.-D., Bartels, A., Schreyer, A. & Clemens, H. (2003). *Textures Microstruct.* **35**, 219–252.

Liss, K.-D., Clemens, H., Bartels, A., Stark, A. & Buslaps, T. (2007*b*). *Proceedings of the Material Research Society Symposium – Advanced Intermetallic-Based Alloys*, edited by C. L. Fu, H. Clemens, J. Wiezorek, M. Takeyama & D. Morris, Warrandale, PA, USA.

Liss, K.-D., Garbe, U., Li, H., Schambron, T., Almer, J. D. & Yan, K. (2009). *Adv. Eng. Mater.* **11**, 637–640.

Liss, K. D., Stark, A., Bartels, A., Clemens, H., Buslaps, T., Phelan, D. & Yeoh, L. A. (2008). *Adv. Eng. Mater.* **10**, 389–392.

Lutterotti, L. (2005). *IUCr CPD Newsl.* **32**, 53–55.

Manchester, F. D. & San-Martin, A. (2000). *Phase Diagrams of Binary Hydrogen Alloys*, edited by F. D. Manchester, pp. 238–258. Materials Park: ASM International.

Paransky, E., Gutmanas, E. Y., Gotman, I. & Koczak, M. (1996). *Metallurg. Mater. Trans. A*, **27**, 2130–2139.

Rawers, J. C. & Wrzesinski, W. R. (1992). *J. Mater. Sci.* **27**, 2877–2886.

San-Martin, A. & Manchester, F. D. (1987). *Bull. Alloy Phase Diag.* **8**, 30–42.

Schuster, J. C. & Palm, M. (2006). *J. Phase Equilib. Diffus.* **27**, 255–277.

Senkov, O. N., Chakoumakos, B., Jonas, J. J. & Froes, F. H. (2001). *Mater. Res. Bull.* **36**, 1431–1440.

Shen, C. C. & Perng, T. P. (2007). *Acta Mater.* **55**, 1053–1058.

Shull, R. D. & Cline, J. P. (1989). *High Temp. Sci.* **26**, 95–117.

Toby, B. H. (2001). *J. Appl. Cryst.* **34**, 210–213.

Valiev, R. Z. & Langdon, T. G. (2006). *Prog. Mater. Sci.* **51**, 881–981.

Wang, Y. M., Chen, M. W., Zhou, F. H. & Ma, E. (2002). *Nature (London)*, **419**, 912–915.

Wasz, M. L., Brotzen, F. R., McLellan, R. B. & Griffin, A. J. Jr (1996). *Int. Mater. Rev.* **41**, 1–12.

Wu, X. & Xia, K. (2006). *Mater. Sci. Forum*, **503–504**, 233–237.

Xia, K. & Wu, X. (2005). *Scr. Mater.* **53**, 1225–1229.

Xu, W., Honma, T., Wu, X., Ringer, S. P. & Xia, K. (2007). *Appl. Phys. Lett.* **91**, 031901.

Xu, W., Wu, X., Sadedin, D., Wellwood, G. & Xia, K. (2008). *Appl. Phys. Lett.* **92**, 011924.

Yamaguchi, M., Inui, H. & Ito, K. (2000). *Acta Mater.* **48**, 307–322.

Yang, W. Y. & Weatherly, G. C. (1996). *J. Mater. Sci.* **31**, 3707–3713.

Yeoh, L. A. & Liss, K.-D. (2006). *dataRring.* Lucas Heights, Australia: Bragg Institute, ANSTO.

Yeoh, L. A., Liss, K.-D., Bartels, A., Chladil, H. F., Avdeev, M., Clemens, H., Gerling, R. & Buslaps, T. (2007). *Scr. Mater.* **57**, 1145–1148.

Zhang, D. L. (2004). *Prog. Mater. Sci.* **49**, 537–560.